Physica Medica 45 (2018) 35–43

Contents lists available at ScienceDirect

Physica Medica

journal homepage: www.elsevier.com/locate/ejmp

Original paper

Occupational exposures during abdominal fluoroscopically guided interventional procedures for different patient sizes — A Monte Carlo approach

William S. Santos[a], Walmir Belinato[b], Ana P. Perini[a,c], Linda V.E. Caldas[c], Diego C. Galeano[d], Carla J. Santos[e], Lucio P. Neves[a,c,e,*]

[a] Instituto de Física, Universidade Federal de Uberlândia (INFIS/UFU), Uberlândia, MG, Brazil
[b] Instituto Federal da Bahia (IFBA), Vitória da Conquista, BA, Brazil
[c] Instituto de Pesquisas Energéticas e Nucleares, Comissão Nacional de Energia Nuclear (IPEN-CNEN/SP), São Paulo, SP, Brazil
[d] Hospital Universitário Júlio Müller, Universidade Federal de Mato Grosso, Cuiabá, MT, Brazil
[e] Programa de Pós-Graduação em Engenharia Biomédica, Faculdade de Engenharia Elétrica, Universidade Federal de Uberlândia, MG, Brazil

ARTICLE INFO

Keywords:
Interventional radiology
Computational dosimetry
Virtual anthropomorphic phantoms

ABSTRACT

In this study we evaluated the occupational exposures during an abdominal fluoroscopically guided interventional radiology procedure. We investigated the relation between the Body Mass Index (BMI), of the patient, and the conversion coefficient values (CC) for a set of dosimetric quantities, used to assess the exposure risks of medical radiation workers. The study was performed using a set of male and female virtual anthropomorphic phantoms, of different body weights and sizes. In addition to these phantoms, a female and a male phantom, named FASH3 and MASH3 (reference virtual anthropomorphic phantoms), were also used to represent the medical radiation workers. The CC values, obtained as a function of the dose area product, were calculated for 87 exposure scenarios. In each exposure scenario, three phantoms, implemented in the MCNPX 2.7.0 code, were simultaneously used. These phantoms were utilized to represent a patient and medical radiation workers. The results showed that increasing the BMI of the patient, adjusted for each patient protocol, the CC values for medical radiation workers decrease. It is important to note that these results were obtained with fixed exposure parameters.

1. Introduction

Some of the factors that contribute to an increasing number of Fluoroscopically Guided Interventional Radiology Procedures (FGIP), carried out in recent years, are related to advances in the image acquisition techniques and the increasing number of experts [1]. Moreover, advances arising from this technique allowed more complex procedures. Thus the option to avoid a surgical procedure brings benefits to critically ill patients, and also reduces the hospital stay time. Despite the benefits of the FGIP, it is not possible to ignore the risks for patients and medical radiation workers.

One of the abdominal FGIP is the percutaneous transhepatic biliary drainage (PTBD) procedure. It is used to drain the bile ducts in the presence of a blockage or damage, that prevents the normal biliary drainage. This is a medical technique that uses fluoroscopic images obtained with X radiation to access the treatment site, usually using a guide catheter for percutaneous or other access, accompanied by a contrast medium to view the organs and radiolucent structures.

During an interventional radiology procedure, patients and medical radiation workers may receive high doses of radiation in their organs and tissues. One of the reasons is the long duration of these procedures. In the case of the medical staff, another reason is the proximity of these professionals in relation to the patients (center of scattered radiation), which emit radiation in different directions, reaching various parts of their bodies. The doses involved in these procedures may vary a lot. The factors that influence these doses are: irradiation geometry, energy spectra, thickness of the examined area, field size, use of personal protective equipment (PPE) and also professional experience.

The direct determination of the doses in organs and tissues of patients and medical staff, during clinical procedures, is a difficult task for most situations. In the literature, it is common to express the results of doses in organs and tissues by a ratio between the estimated, or

* Corresponding author at:Instituto de Física, Universidade Federal de Uberlândia (INFIS/UFU), Uberlândia, MG, Brazil.
E-mail addresses: william@ufu.br (W.S. Santos), wbfisica@gmail.com (W. Belinato), anapaula.perini@ufu.br (A.P. Perini), lcaldas@ipen.br (L.V.E. Caldas), galeano@fisica.ufmt.br (D.C. Galeano), carlaafro@yahoo.com.br (C.J. Santos), lucio.neves@ufu.br (L.P. Neves).

https://doi.org/10.1016/j.ejmp.2017.11.016
Received 24 July 2017; Received in revised form 21 November 2017; Accepted 24 November 2017

measured dosimetric quantity, by another quantity, which can be obtained more easily by experimental arrangements, such as, for example, the dose area product (DAP). The result of this ratio is called dose conversion coefficient (CC), which is a function of the field and radiation source parameters (X-ray tube voltage, filtration, field size, field position, focus-skin distance, etc.). This ratio depends also on the anatomical properties of the anthropomorphic phantoms, such as the elementary composition of relevant tissues of the body, and the applied radiation transport method. Thus, dosimetric measurements can be interpreted in terms of absorbed dose, by multiplying the value obtained from the instrument by the appropriate CC for exposure situations, similar to the actual exposure.

For consistency, in this study, the estimated doses to organs, and all other evaluated quantities, such as equivalent dose and effective dose, will also be presented in this format.

In the interventional radiology, the published works using Monte Carlo (MC) simulation focused mainly on the protection of workers and patients, involved in cardiac angiography and coronary angioplasty procedures [2–8]. However, to our knowledge, there are no dosimetry studies with MC simulation assessing occupational exposures in PTBD, or any other abdominal procedure. The few data from the literature are related to clinical exposures in patients [1,9–12], and some experimental studies regarding occupational radiation exposure in vascular interventional exams [13,14].

In recent years, the Body Mass Index (BMI) of the population has increased, and the use of virtual anthropomorphic phantoms, with higher body mass to represent a specific patient, is a necessity [15–19]. In addition, to the evaluation of medical exposures, another objective of this paper was to evaluate the influence of patients with higher BMI on occupational exposures. This assessment was made by CC values to effective (CC[E]) and equivalent (CC[H_T]) doses, of patients of different heights and body weights, which are subject to a PTBD procedure. To achieve these goals, a realistic exposure model was created using three virtual anthropomorphic phantoms simultaneously, two medical radiation workers and one patient. Finally, we build the scenarios of the energy fluence maps, that allow the knowledge of the most critical points in the interior of the procedures room.

2. Materials and methods

In this study, we used the adult virtual anthropomorphic phantoms FASH3 and MASH3, to represent the medical radiation workers. They were built on mesh surfaces, at the *Department of Nuclear Energy*, *Federal University of Pernambuco* (UFPE) [16,20]. In this work, we will name the professionals as *main physician* and *assistant physician*, due to their positions in relation to the X-ray tube. However, other professionals may be positioned in their places.

The patients were represented by a set of virtual anthropomorphic phantoms, with different heights and body masses. The images of the virtual anthropomorphic phantoms, and their anthropometric characteristics, are shown in Fig. 1 and Table 1, respectively.

All of the virtual anthropomorphic phantoms used in this study have voxel edges of 0.24 cm long. These virtual anthropomorphic phantoms were coupled to the radiation transport code MCNPX 2.7.0 [21]. This code describes the transport radiation through matter, including photons and electrons, that may be transported individually, or simultaneously photon/electron, in three-dimensional geometry and heterogeneous systems.

In addition to the anthropometric characteristics, we also evaluated the effects of technical parameters, such as tube voltage and angle of the beam on the CC[H_T] and CC[E] to medical radiation workers and patients.

In this study, the CC values were calculated for a set of organs and tissues of dosimetric importance, from three beam projections: posteroanterior (PA), right anterior oblique (RAO25°) and left anterior oblique (LAO25°). In all cases, the radiation beam is focused on the patient's liver, to mimic a PTBD procedure, with fields of view (FOV) of 20 cm × 20 cm and 30 cm × 30 cm. Different FOV were employed in the simulations to evaluate the influence of its size on the CC values. The source-skin distances were set at 60 cm for PA projection, 56 cm for LAO25° and 54 cm for the RAO25° projections. The focus detector distance was 100 cm, 116 cm and 114 cm for the PA, LAO25° and RAO25° projections, respectively.

The X-ray tube was simplified to a point source that emits radiation isotropically, in a solid angle specified by the field size and focal length. The X-ray spectra were generated following the recommendations of the catalogue of X-ray spectra IPEM report number 78 (SR-78 software) [22], which enables the combination of several radiographic parameters. They were: maximum photon energies of 80, 100 and 120 keV, tungsten as target material, anodic angle of 12°, filtration/half-value layer set at 4.0/4.8; 4.7/5.0 and 3.8/5.5 mmAl, with effective energies of 38.8, 44.0 and 45.4 keV, respectively.

In order to make the radiation scenarios as close to reality as possible, the most common objects, present within the intervention room, were modeled, by computational method, to evaluate all effects generated in the medium, such as scattering, absorption and production of secondary particles. In this sense, we built a room of concrete walls and filled with atmospheric air. Within this area, in addition to medical workers and patient, the major components of the X-ray equipment were inserted. The X-ray tube was composed of Pb with a density of 11.35 g/cm^3; and the image intensifier was composed of a CsI crystal, with a density of 1.25 g/cm^3 (composition: Cs (50%), I (50%)); Al_2O_3 substrate, density of 1.25 g/cm^3 (composition: Al (40%), O (60%)) and a shield, with density of 7.87 g/cm^3 (composition: Mn (0.5%), Fe (99.5%)).

A 15 cm thick surgical table made of carbon fiber with a metal base was also modeled. It had a density of 1.25 g/cm^3 and a composition of: H (5.7441%), C (77.4591%) and O (16.7968%). The table was positioned at a height of 90 cm from the room floor. Two medical radiation workers were positioned at the right side of the surgical table, at the level of the patient's groin, and in front of a video monitoring system.

We also simulated an ionization chamber, filled with atmospheric air to measure the DAP. In all situations the ionization chamber was positioned 15 cm from the focal spot. The ionization chamber's size was modeled in such a way that its dimensions would be compatible to those of the X-ray beam. For the 20 cm FOV the dimensions were (5 × 5 × 1) cm^3 and for the 30 cm FOV (15 × 15 × 1) cm^3. With those dimensions, the ionization chamber was within the area perpendicular to the X-ray beam.

Fig. 2 shows the computational exposure scenario with three virtual anthropomorphic phantoms, representing the patient and medical radiation workers, involved in PTBD procedures. In this figure, the PPE, and other typical components of an interventional radiology room were also included.

The PPE, used by medical radiation workers, were carefully modeled. These devices are generally made of 0.5 mm thick lead equivalent in front of the operator. Among the most important equipment are the apron, thyroid shield and lead eyewear (composed by lead glass). This apron model is 1.20 m long and 55 cm wide, extending from the chest level until the region of the knees, with the sides of the shoulders and arms of the workers exposed. The lead eyewear, shaped as glasses, was also inserted, as well as the thyroid shield, with a ring shape, covering the entire neck. The suspended curtain and lead glass shields with equivalent thickness of 0.5 mm lead were also inserted. These devices are often used for the protection of radiation workers who are exposed to the primary radiation beam, and especially the scattered radiation from the patient and the surgical table.

The absorbed doses in the main radiosensitive organs and tissues, of the male and female virtual anthropomorphic phantoms, were determined considering the energy deposited in the region of interest of all primary and secondary radiation. Since the w_R weighting factor for photons is 1, the absorbed dose is numerically equal to the equivalent

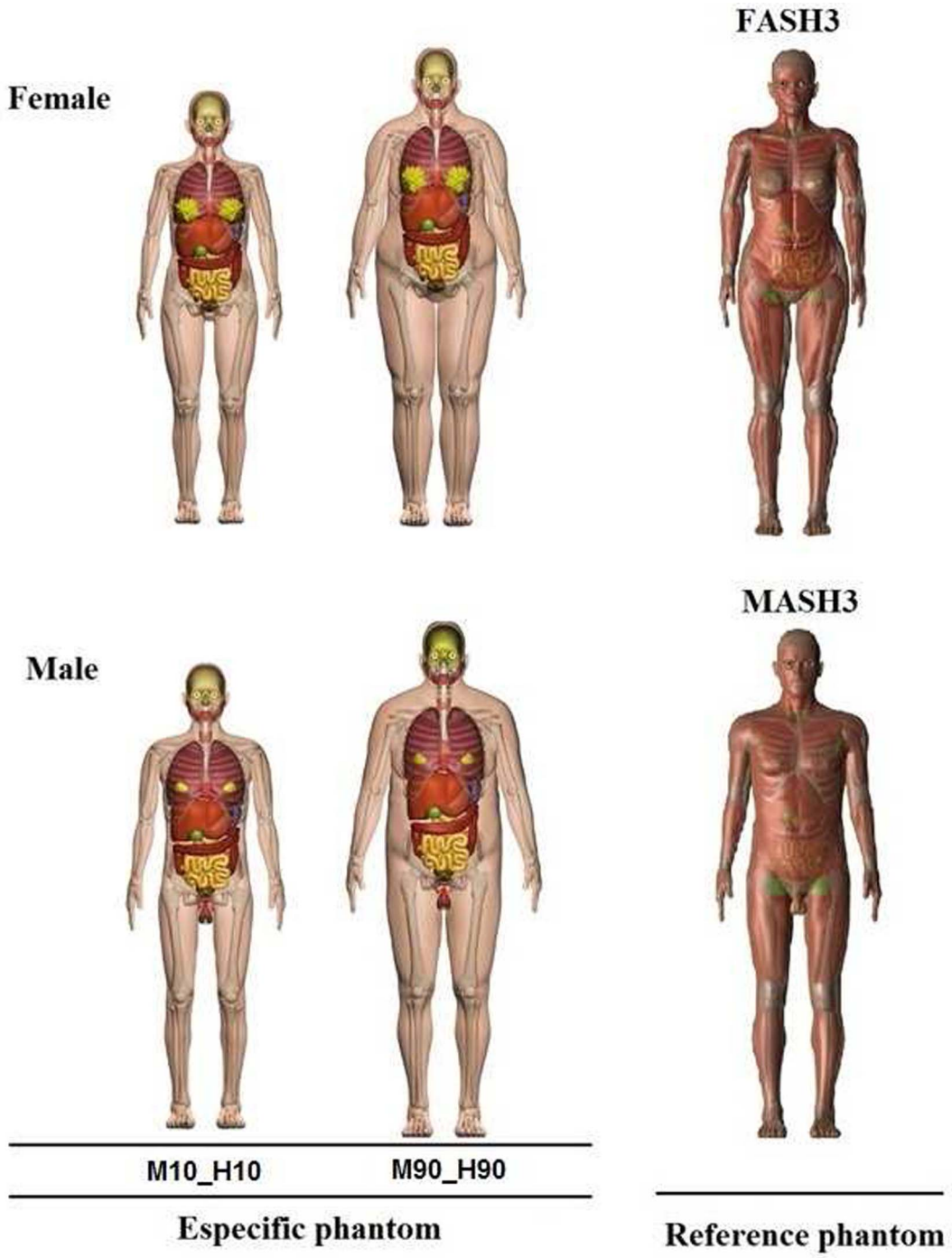

Fig. 1. Front view of female and male virtual anthropomorphic phantoms, with mass percentage and height of 10 and 90th, used to represent the patient. It also shows the MASH3 and FASH3 reference virtual anthropomorphic phantoms, used to represent the radiation medical workers.

Table 1
Some important properties of the female and male virtual anthropomorphic phantoms used in this study.

Phantoms	Mass and height percentage	Mass (kg)	Height (cm)	Matrix (columns × lines × slices)	BMI (kg/m^2)	Waist circumference (cm)
Male	M10_H10	59.3	167.3	238 × 129 × 697	21.2	81.8
	M90_H90	108.5	185.6	298 × 148 × 773	31.5	110.4
Reference Male	MASH3	73.0	176.0	239 × 129 × 731	23.6	–
Female	M10_H10	48.6	155.5	219 × 124 × 648	20.1	70.7
	M90_H90	94.0	172.2	271 × 141 × 718	31.7	100.9
Reference Female	FASH3	60.0	163.0	221 × 128 × 677	22.7	–

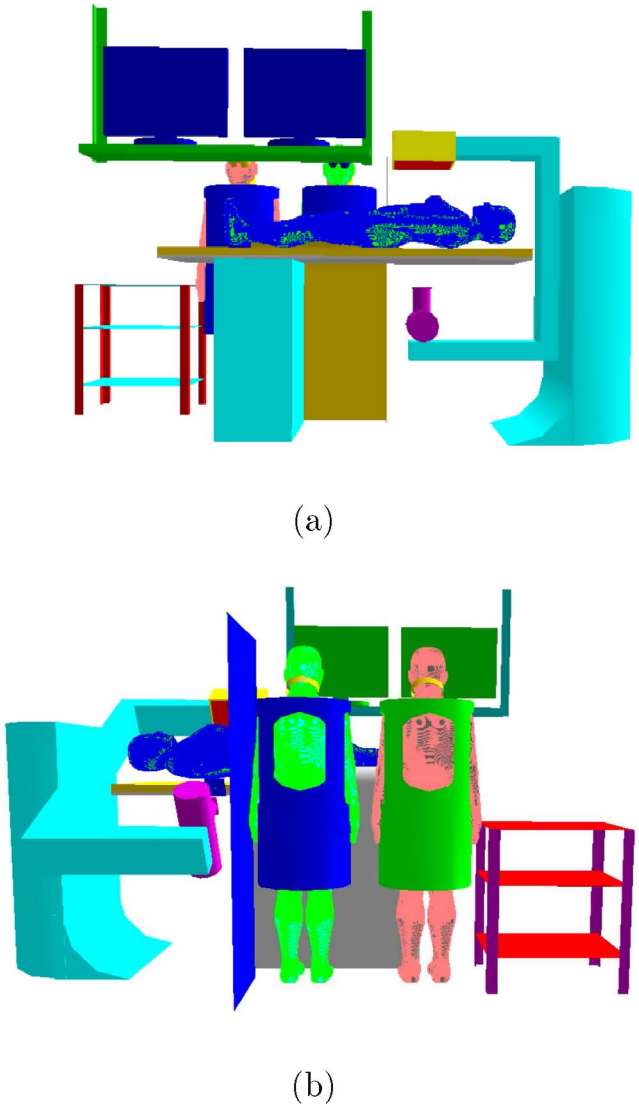

Fig. 2. Irradiation scenario modeled with the MCNPX code, consisting of three virtual anthropomorphic phantoms, representing a main physician, an assistant physician and a patient in: (a) PA projection and (b) LAO25° projection.

dose. The w_T weighting factors of each organ and tissue, recommended by ICRP 103 [23], were applied to the CC[H_T] of each organ and tissue, in order to determine the CC[E] values. They were calculated using Eq. 1 [24].

$$CC[E] = \sum_T w_T \left[\frac{CC[H_T]_{T,Male} + CC[H_T]_{T,Female}}{2} \right] \quad (1)$$

where w_T is the weighting factor for each organ and tissue, $CC[H_T]_{T,Male}$ is the conversion factor for male virtual anthropomorphic phantom and $CC[H_T]_{T,Female}$ for the female virtual anthropomorphic phantom.

In experimental evaluations, sometimes, it is not possible to determine the equivalent doses taking into account the male and female radiation workers (or patients). In these cases, the evaluation is carried out with only one gender. In order to allow a better comparison with the data presented in this work, we decided to present a complete list of CC[H_T] and also the equivalent dose, normalized by the DAP, for each gender (named $(E/DAP)_{Male}$ and $(E/DAP)_{Female}$). These results are presented at the Supplementary Material of this paper.

To estimate the deposited dose in the radiosensitive organs and tissues, represented in each virtual anthropomorphic phantom, we used the *F6* tally (MeV/g) of the MCNPX code, with the exception of the red bone marrow (RBM) and the skeleton, where we used the tally energy fluence $^{*}F4$ (MeV/cm^2). In the energy range of diagnostic radiology, the *F6* tally provides the energy deposition. The tally values were then normalized by the DAP.

The bones of the virtual anthropomorphic phantoms, used in this study, were modeled as a homogeneous mixture of bone mineral and organic constituent of the skeleton, including active bone marrow. The overall composition of the skeleton is approximated as being uniform in all bones in the body, but the amount of active bone marrow varies from one part to another of the skeleton. In fact, the active bone marrow is located in small cavities in the trabecular bone, and in this case it is necessary to use the correction factors to calculate the dose. In this sense, the determination of the energy absorbed by the red bone marrow is done by applying three correction factors described in Eq. (2) [24],

$$E_{RBM} = E_{HB} * \frac{m_{RBM}}{m_{HB}} * \frac{\left(\frac{\mu_{en}(E)}{\rho}\right)_{RBM}}{\left(\frac{\mu_{en}(E)}{\rho}\right)_{HB}} * S(E) \quad (2)$$

where E_{HB} is the energy deposited in the homogeneous bone of the skeleton. m_{RBM} and m_{HB} denote the masses of the part of the skeleton and of the bone marrow, respectively. E is the energy of the incident photon and $\mu_{en}(E)/\rho$ is the mass-energy absorption coefficient.

The influence of the size of the cavity, of the active bone marrow, on the dose is considered by the dose intensification factor, $S(E)$ [25]. It is noted that dividing both sides of Eq. (3) by the mass of RBM skeletal site, Eq. (1) can be rewritten in terms of the absorbed dose to RBM [24],

$$D_{RBM} = D_{HB} * \frac{\left(\frac{\mu_{en}(E)}{\rho}\right)_{RBM}}{\left(\frac{\mu_{en}(E)}{\rho}\right)_{HB}} * S(E) \quad (3)$$

where D_{HB} is the absorbed dose by the homogeneous bone skeleton. It is calculated multiplying the energy fluence (Ψ_{HB}) in the skeleton by the $\mu_{en}(E)/\rho$, as described in Eq. (4) [24]. The dose in the bone surface was approximated as being the dose to the homogeneous bone, which was calculated on the basis of particle equilibrium conditions.

$$D_{RBM} = \Psi_{HB} * \left(\frac{\mu_{en}(E)}{\rho}\right)_{RBM} * S(E) \quad (4)$$

The values of the mass-energy absorption coefficients and of the intensification factors were extracted from the publication ICRP 116 [25]. They were prepared in an input file to the MCNPX using the cards DE (energy function) and DF (response function), utilizing the energy fluence tally $^{*}F4$. Thus, the absorbed doses in RBM and homogeneous bone were calculated directly during the simulation, as the DE and DF cards allow conversion of energy fluence values for the corresponding dose values, by log-log interpolation. The number of particle histories (1.0E9) was chosen to reduce statistical uncertainties. All parameters of the particle transport, and cross section libraries, were kept at their default values.

3. Results and discussion

In this section we will present how a change in the radiographic technique, used to adjust the BMI of the patient, may affect occupational exposures.

The CC[H_T] were calculated in specific ways, depending on the region, as follows:

- the male breasts were made considering that the body phantom is composed of a thin layer of voxel;
- the doses in the testicles and ovary were used to calculate the CC[H_T] in the gonads;
- the colon was considered as being the lower part of the large

Table 2
CC[H_T] and $(E/DAP)_{Male}$ ($\mu Sv/Gy.\ cm^2$) for the male main physician, with a 30 cm FOV. In this table only the organs with the higher CC[H_T] values are presented. The complete data, for all organs, projections and FOV are presented at the Supplementary Material of this paper.

Organs	M10_H10			M90_H90		
	PA	RAO25°	LAO25°	PA	RAO25°	LAO25°
Tube voltage of 80 kVp						
Bone marrow	9.8E−02	1.1E−01	1.2E−01	5.8E−02	4.3E−02	9.2E−02
Thyroid	5.4E−02	9.4E−02	1.4E−01	2.6E−02	5.0E−02	3.3E−02
Brain	1.0E−01	1.5E−01	1.0E−01	4.1E−02	3.1E−02	6.0E−02
Salivary glands	6.7E−02	8.7E−02	8.5E−02	3.1E−02	2.5E−02	3.9E−02
Skin	8.1E−02	8.2E−02	1.0E−01	6.3E−02	4.4E−02	9.8E−02
Eye lens	5.1E−01	4.7E−01	4.3E−01	2.0E−01	1.1E−01	2.3E−01
$(E/DAP)_{Male}$	3.1E−02	3.2E−02	4.3E−02	1.9E−02	1.4E−02	3.3E−02
Tube voltage of 100 kVp						
Bone marrow	2.0E−01	2.0E−01	2.6E−01	1.2E−01	8.5E−02	2.1E−01
Thyroid	1.2E−01	1.7E−01	2.3E−01	6.0E−02	8.8E−02	7.3E−02
Brain	2.2E−01	2.7E−01	2.3E−01	9.8E−02	6.3E−02	1.4E−01
Salivary glands	1.3E−01	1.5E−01	1.5E−01	6.1E−02	4.2E−02	8.1E−02
Skin	1.4E−01	1.3E−01	2.0E−01	1.1E−01	7.9E−02	1.9E−01
Eye lens	8.4E−01	7.8E−01	8.2E−01	3.7E−01	2.1E−01	4.6E−01
$(E/DAP)_{Male}$	7.7E−02	6.4E−02	1.1E−01	5.2E−02	3.3E−02	9.3E−02
Tube voltage of 120 kVp						
Bone marrow	2.6E−01	2.5E−01	3.7E−01	1.7E−01	1.1E−01	3.2E−01
Thyroid	1.6E−01	2.0E−01	3.0E−01	9.2E−02	1.0E−01	1.2E−01
Brain	2.9E−01	3.4E−01	3.1E−01	1.3E−01	8.3E−02	2.0E−01
Salivary glands	1.6E−01	1.8E−01	1.9E−01	7.9E−02	5.7E−02	1.1E−01
Skin	1.8E−01	1.6E−01	2.7E−01	1.4E−01	9.7E−02	2.7E−01
Eye lens	1.0E + 00	9.4E−01	9.9E−01	4.7E−01	2.6E−01	6.0E−01
$(E/DAP)_{Male}$	1.1E−01	8.4E−02	1.8E−01	8.0E−02	4.6E−02	1.6E−01

Table 3
CC[H_T] and $(E/DAP)_{Male}$ ($\mu Sv/Gy.\ cm^2$) for the male assistant physician, with a 30 cm FOV. In this table only the organs with the higher CC[H_T] values are presented. The complete data, for all organs, projections and FOV are presented at the Supplementary Material of this paper.

Organs	M10_H10			M90_H90		
	PA	RAO25°	LAO25°	PA	RAO25°	LAO25°
Tube voltage of 80 kVp						
Bone marrow	1.1E−01	7.2E−02	9.8E−02	6.5E−02	2.7E−02	5.6E−02
Thyroid	5.8E−02	8.9E−02	9.4E−02	3.4E−02	4.8E−02	3.4E−02
Brain	1.7E−01	1.1E−01	1.4E−01	8.2E−02	2.7E−02	6.4E−02
Salivary glands	1.1E−01	5.9E−02	1.0E−01	6.2E−02	2.2E−02	4.9E−02
Skin	6.4E−02	5.4E−02	6.5E−02	4.3E−02	2.6E−02	4.5E−02
Eye lens	3.9E−01	2.0E−01	3.2E−01	1.6E−01	6.0E−02	1.4E−01
$(E/DAP)_{Male}$	3.6E−02	2.2E−02	3.4E−02	2.4E−02	9.7E−03	2.7E−02
Tube voltage of 100 kVp						
Bone marrow	1.8E−01	1.2E−01	1.6E−01	1.0E−01	4.7E−02	9.6E−02
Thyroid	1.0E−01	1.3E−01	1.5E−01	6.0E−02	6.9E−02	6.2E−02
Brain	2.9E−01	1.9E−01	2.5E−01	1.4E−01	4.9E−02	1.2E−01
Salivary glands	1.6E−01	9.3E−02	1.6E−01	8.5E−02	3.7E−02	7.7E−02
Skin	9.2E−02	8.0E−02	9.7E−02	6.2E−02	4.1E−02	6.9E−02
Eye lens	5.4E−01	3.3E−01	5.0E−01	2.3E−01	1.1E−01	2.5E−01
$(E/DAP)_{Male}$	6.0E−02	3.7E−02	5.9E−02	3.9E−02	1.7E−02	4.8E−02
Tube voltage of 120 kVp						
Bone marrow	2.1E−01	1.4E−01	1.9E−01	1.2E−01	5.6E−02	1.2E−01
Thyroid	1.3E−01	1.7E−01	1.8E−01	7.9E−02	8.4E−02	8.0E−02
Brain	3.4E−01	2.3E−01	3.1E−01	1.7E−01	6.2E−02	1.6E−01
Salivary glands	1.8E−01	1.1E−01	1.8E−01	9.6E−02	4.1E−02	9.1E−02
Skin	1.0E−01	8.9E−02	1.1E−01	7.0E−02	4.7E−02	7.9E−02
Eye lens	6.6E−01	4.0E−01	5.9E−01	2.8E−01	1.3E−01	3.2E−01
$(E/DAP)_{Male}$	7.3E−02	4.5E−02	7.3E−02	4.8E−02	2.0E−02	5.9E−02

intestine;

- other organs were calculated taking into account the equivalent doses in the adrenal glands, extrathoracic region (larynx + pharynx), gallbladder wall, kidneys, lymph nodes, muscles, heart, oral mucosa, pancreas, prostate (men), the wall of the small intestine, spleen, thymus and uterus (female), as recommended by the ICRP 103 [23].

3.1. Evaluation of the CC[H_T] and CC[E] to medical radiation workers as a function of the patient's BMI

In Table 2 the organs with the higher CC[H_T] values are shown, for the main physician, during the exam of the M10_H10 and M90_H90 virtual anthropomorphic phantoms, with a 30 cm FOV. Similarly, the main results for the assistant physician are shown in

Table 4
CC[E] and average CC[E] (per procedure) for main and assistant physicians, with 20 cm and 30 cm FOV, during procedures with the M10_H10 and M90_H90 phantoms.

Tube voltage (kV)	CC[E] (μSv/Gy.cm^2) – 20 cm×20 cm FOV				CC[E] (μSv/Gy.cm^2) – 30 cm×30 cm FOV			
	PA	RAO25°	LAO25°	Average	PA	RAO25°	LAO25°	Average
MAIN PHYSICIAN – M10_H10								
80	2.3E−02(3%)	1.9E−02(3%)	3.2E−02(2%)	1.9E−1(1%)	3.3E−02(2%)	3.5E−02(2%)	4.3E−02(2%)	2.5E−1(1%)
100	6.2E−02(1%)	4.3E−02(1%)	8.5E−02(1%)		8.0E−02(1%)	7.0E−02(1%)	1.1E−01(1%)	
120	9.4E−02(1%)	5.9E−02(1%)	1.5E−01(1%)		1.2E−01(1%)	9.1E−02(1%)	1.8E−01(1%)	
ASSISTANT PHYSICIAN – M10_H10								
80	2.9E−02(5%)	1.3E−02(7%)	3.3E−02(6%)	1.2E−1(4%)	3.5E−02(5%)	2.2E−02(4%)	3.6E−02(5%)	1.5E−1(3%)
100	4.9E−02(4%)	2.4E−02(5%)	5.8E−02(4%)		5.8E−02(3%)	3.6E−02(3%)	6.0E−02(3%)	
120	6.0E−02(3%)	3.0E−02(4%)	7.3E−02(3%)		7.1E−02(2%)	4.3E−02(3%)	7.4E−02(2%)	
MAIN PHYSICIAN – M90_H90								
80	1.5E−02(3%)	8.7E−03(4%)	2.5E−02(2%)	1.3E−1(1%)	2.0E−02(2%)	1.4E−02(2%)	3.4E−02(2%)	1.8E−1(1%)
100	4.1E−02(1%)	2.1E−02(2%)	7.0E−02(1%)		5.3E−02(1%)	3.2E−02(1%)	9.5E−02(1%)	
120	6.5E−02(1%)	3.1E−02(2%)	1.2E−01(1%)		8.0E−02(1%)	4.5E−02(1%)	1.6E−01(1%)	
ASSISTANT PHYSICIAN – M90_H90								
80	1.8E−02(5%)	6.1E−03(7%)	2.5E−02(5%)	7.9E−2(4%)	2.2E−02(4%)	8.6E−03(6%)	2.5E−02(4%)	8.8E−2(3%)
100	3.0E−02(4%)	1.1E−02(7%)	4.3E−02(4%)		3.6E−02(3%)	1.5E−02(3%)	4.3E−02(2%)	
120	3.6E−02(3%)	1.4E−02(4%)	5.3E−02(3%)		4.4E−02(2%)	1.8E−02(3%)	5.2E−02(2%)	

Table 5
$CC[H_T]$ and $(E/DAP)_{Male}$ (mSv/Gy. cm^2) for the male patient, with a 30 cm FOV. In this table only the organs with the higher $CC[H_T]$ values are presented. The complete data, for all organs, projections and FOV are presented at the Supplementary Material of this paper.

Organs	M10_H10			M90_H90		
	PA	RAO25°	LAO25°	PA	RAO25°	LAO25°
Tube voltage of 80 kVp						
Bone marrow	1.0E−01	1.2E−01	1.2E−01	6.7E−02	5.1E−02	5.8E−02
Colon	7.2E−02	1.3E−01	6.1E−02	3.1E−02	5.8E−02	2.0E−02
Lung	2.7E−01	1.7E−01	2.0E−01	1.9E−01	1.0E−01	1.1E−01
Oesophagus	1.3E−01	1.3E−01	1.5E−01	9.8E−02	7.1E−02	7.3E−02
Liver	2.4E−01	7.0E−02	3.7E−01	1.4E−01	3.7E−02	1.8E−01
Skin	9.6E−02	1.3E−01	1.3E−01	7.6E−02	1.1E−01	1.1E−01
$(E/DAP)_{Male}$	8.3E−02	7.4E−02	8.2E−02	5.0E−02	3.4E−02	3.6E−02
Tube voltage of 100 kVp						
Bone marrow	1.4E−01	1.5E−01	1.5E−01	9.3E−02	7.3E−02	8.1E−02
Colon	1.1E−01	1.7E−01	8.7E−02	4.9E−02	8.4E−02	3.2E−02
Lung	3.6E−01	2.3E−01	2.7E−01	2.6E−01	1.5E−01	1.5E−01
Oesophagus	2.0E−01	2.0E−01	2.1E−01	1.5E−01	1.1E−01	1.1E−01
Liver	3.4E−01	1.1E−01	5.0E−01	2.1E−01	6.3E−02	2.6E−01
Skin	1.1E−01	1.5E−01	1.5E−01	8.6E−02	1.2E−01	1.2E−01
$(E/DAP)_{Male}$	1.1E−01	1.0E−01	1.1E−01	7.2E−02	4.9E−02	5.3E−02
Tube voltage of 120 kVp						
Bone marrow	1.5E−01	1.6E−01	1.6E−01	1.0E−01	8.0E−02	8.8E−02
Colon	1.2E−01	1.9E−01	9.7E−02	5.7E−02	9.3E−02	3.7E−02
Lung	3.8E−01	2.5E−01	2.9E−01	2.8E−01	1.6E−01	1.7E−01
Oesophagus	2.3E−01	2.2E−01	2.4E−01	1.8E−01	1.3E−01	1.3E−01
Liver	3.8E−01	1.3E−01	5.4E−01	2.4E−01	7.6E−02	2.9E−01
Skin	1.1E−01	1.5E−01	1.5E−01	8.8E−02	1.3E−01	1.3E−01
$(E/DAP)_{Male}$	1.3E−01	1.1E−01	1.2E−01	8.0E−02	5.5E−02	5.9E−02

Table 6
CC[E] and average CC[E] (per procedure) for the the M10_H10 and M90_H90 patients, with 20 cm and 30 cm FOV.

Tube voltage (kV)	CC[E] (mSv/Gy.cm^2) – 20 cm × 20 cm FOV				CC[E] (mSv/Gy.cm^2) – 30 cm × 30 cm FOV			
	PA	RAO25°	LAO25°	Average	PA	RAO25°	LAO25°	Average
PATIENT – M10_H10								
80	7.9E−02(0.1%)	8.7E−02(0.1%)	1.1E−01(0.1%)	3.5E−1(0.1%)	9.6E−02(0.1%)	9.0E−02(0.1%)	1.0E−01(0.1%)	3.7E−1(0.1%)
100	1.1E−01(0.1%)	1.2E−01(0.1%)	1.5E−01(0.1%)		1.3E−01(0.1%)	1.2E−01(0.1%)	1.4E−01(0.1%)	
120	1.2E−01(0.1%)	1.3E−01(0.1%)	1.6E−01(0.1%)		1.4E−01(0.1%)	1.3E−01(0.1%)	1.5E−01(0.1%)	
PATIENT – M90_H90								
80	4.8E−02(0.1%)	4.0E−02(0.1%)	4.9E−02(0.1%)	1.9E−1(0.1%)	5.5E−02(0.1%)	4.1E−02(0.1%)	4.3E−02(0.1%)	1.9E−1(0.1%)
100	7.0E−02(0.1%)	5.9E−02(0.1%)	7.0E−02(0.1%)		7.9E−02(0.1%)	5.8E−02(0.1%)	6.1E−02(0.1%)	
120	7.9E−02(0.1%)	6.5E−02(0.1%)	7.8E−02(0.1%)		8.8E−02(0.1%)	6.5E−02(0.1%)	6.8E−02(0.1%)	

Table 7
Percentage decrease of dose with PPE to the medical radiation workers for the PA, RAO25° and LAO25° projections, using a tube voltage of 120 kVp and M90_H90 patient phantom, and 30 cm FOV.

PPE	$(E/DAP)_{Male}$ or $CC[H_T]$	Percentage decrease of dose with PPE		
		PA	RAO25°	LAO25°
Main Physician – Male				
Lead eyewear	$CC[H_{Eye\ lens}]$	13	31	12
Lead eyewear and lead glass shields	$CC[H_{Eye\ lens}]$	66	50	80
Lead apron	$(E/DAP)_{Male}$	89	79	86
	$CC[H_{Lung}]$	89	80	78
	$CC[H_{Stomach}]$	90	85	91
	$CC[H_{Breast}]$	95	93	94
	$CC[H_{Gonads}]$	81	80	90
	$CC[H_{Liver}]$	91	89	93
Thyroid shield	$CC[H_{Thyroid}]$	13	14	12
Lead curtain	$(E/DAP)_{Male}$	69	73	41
Lead glass shields	$(E/DAP)_{Male}$	68	52	80
Assistant Physician – Male				
Lead eyewear	$CC[H_{Eye\ lens}]$	18	39	19
Lead eyewear and lead glass shields	$CC[H_{Eye\ lens}]$	31	43	59
Lead apron	$(E/DAP)_{Male}$	74	74	79
	$CC[H_{Stomach}]$	78	85	81
	$CC[H_{Breast}]$	96	96	96
	$CC[H_{Gonads}]$	88	96	96
	$CC[H_{Bladder}]$	83	88	89
	$CC[H_{Liver}]$	87	92	89
Thyroid shield	$CC[H_{Thyroid}]$	14	18	21
Lead curtain	$(E/DAP)_{Male}$	74	73	67
Lead glass shields	$(E/DAP)_{Male}$	11	9	30

Table 3, also for a 30 cm FOV. The complete data are shown at the Supplementary Material of this paper. The results for the female medical workers, using a FOV of 20 cm are presented in Tables 8–10; and for a FOV of 30 cm are presented in Tables 11–13. The results for the male radiation workers are presented in Tables 14–16 (20 cm FOV), 17–19 (30 cm FOV).

As stated before, we used 1.0E9 particle histories, to reduce the statistical uncertainties. This was achieved for all studied organs, with only some of the smaller and out-of-field organs (i.e., gonads and bladder), where it is possible to observe large uncertainties. The gonads and bladder are small organs, surrounded by other tissues, which increased the uncertainties, for the medical workers (exposed only for the scattered radiation). This fact was not observed for the patients, exposed to the direct beam, and in their cases the uncertainties for these organs were much lower.

As it can be observed in Tables 2 and 3, with some exceptions, the general trend for $CC[H_T]$ to medical radiation workers is to be inversely related to the patient's BMI. When the patient's BMI increases, the $CC[H_T]$, and also the $(E/DAP)_{Male}$, decreases. This was observed for both genders in all scenarios evaluated in this work. Comparing the $(E/DAP)_{Female}$ and $(E/DAP)_{Male}$ (presented at the Supplementary Material), we observed that the highest difference was up to 16% (30 cm FOV, 80 kVp) for the main physician and 36% (20 cm FOV, 120 kVp) for the assistant physician.

Table 4 shows the CC[E], and average CC[E], which is the average of the CC[E] per procedure, to the medical radiation workers. We may notice that the CC[E] values are lower for the M90_H90 phantoms, when comparing them to the M10_H10 for all cases.

This may be explained by the increase of organ and tissue masses, which reduces the photon attenuation. Thus, the scattered radiation to the medical workers will decrease. Nevertheless, it is important to note that the results were obtained with fixed exposure parameters, while in the actual functioning of the equipment, a BMI increase is usually associated to an automatic exposure control. If we compare M10_H10 values at 80 kVp with M90_H90 at 100 kVp, we can observe higher CC[E] values for the M90_H90, and these parameters are compatible with the clinical situation.

The increase in body mass leads to an increase in the adipose tissue, surrounding the internal organs, and in the abdominal region of the patient. This provides additional material to radiation scattering, causing a decrease in the CC[E] values of the organs and other structures of the radiation medical workers.

The LAO25° projection was considered as the most critical, for medical professionals, compared with the PA and RAO25° projections. In the LAO25° projection, the physician has higher values due to his/her positioning towards the primary radiation beam, and to the scattered radiation center. It is important to note, however, that in the actual clinical situation the position of the assistant is usually not fixed and stable, as the one of the first operator. Also from a radiation protection point of view, the assistant physician may position himself "one step back", and this result in a significant dose reduction. All these factors were not considered during the simulation, where we decided to investigate the cases with the highest dose values. On the other hand, if this professional stays in this position, this study suggests that an additional extra protection, for this professional, should be evaluated. Another issue is the tube voltage. When the voltage increases, the $CC[H_T]$ and CC[E] also increase.

Furthermore, from Table 4 we may notice that an increase in the FOV size, from 20 cm to 30 cm, leads to an increase in the average CC[E]. For the main physician, the increase was up to 28%, while for the assistant physician the increase was 20%. The scattering radiation from the patient increases with increasing FOV, thus leading to an increase in the CC[E] to the medical professionals.

Our results are based on Monte Carlo simulations, without experimental validations, and from our point of view, a comparison with experimental data is a very important task. To compare our results with those from the literature, we determined the average CC[E], for the main and assistant physicians, considering a 20 cm FOV. The average CC[E] for the main physician was 0.19 $\mu Sv/Gy.\ cm^2$, with the M10_H10 phantom representing the patient undergoing the procedure, and 0.13 $\mu Sv/Gy.\ cm^2$ for the M90_H90 phantom. The average CC[E] for the assistant physician was 0.12 $\mu Sv/Gy.\ cm^2$ (M10_H10 phantom) and 0.079 $\mu Sv/Gy.\ cm^2$ (M90_H90 phantom). The same trend was observed for both physicians: an increase on the BMI of the patient leads to a decrease in the CC[E] values.

These results are in agreement with those from the literature, as in the work of Tsapaki et al. [26], with a value of 0.132 $\mu Sv/Gy.\ cm^2$ for coronary angiography procedures, and 0.168 $\mu Sv/Gy.\ cm^2$ for percutaneous transluminal coronary angioplasty procedures. Our results are also in agreement with those from Bor et al. [27], who presented an average value of 0.14 $\mu Sv/Gy.\ cm^2$ for medical radiation workers of angiographic units (rage: 0.02–0.42).

The mean values of the ratio between lens doses (estimated from the chest dosemeter) and KAP (0.21 – 0.46 $\mu Sv/Gy.\ cm^2$) were obtained in the work of Vano et al. [28]. Our results are in agreement with these results too. Values of ratio E/DAP for complete procedures in X-ray procedures of radiology, cardiology and other clinical staff, were discussed in the work of Martin [29]. These values were between 0.006 $\mu Sv/Gy.\ cm^2$ and 0.2 $Sv/Gy.\ cm^2$. It is possible to observe that our results are within this interval. The work of Trianni et al. [30] discussed the effective dose normalized to DAP to cardiologist reported in the literature for different types of cardiac interventional exams. These results were between 0.021 and 0.054 $\mu Sv/Gy.\ cm^2$. These results are lower

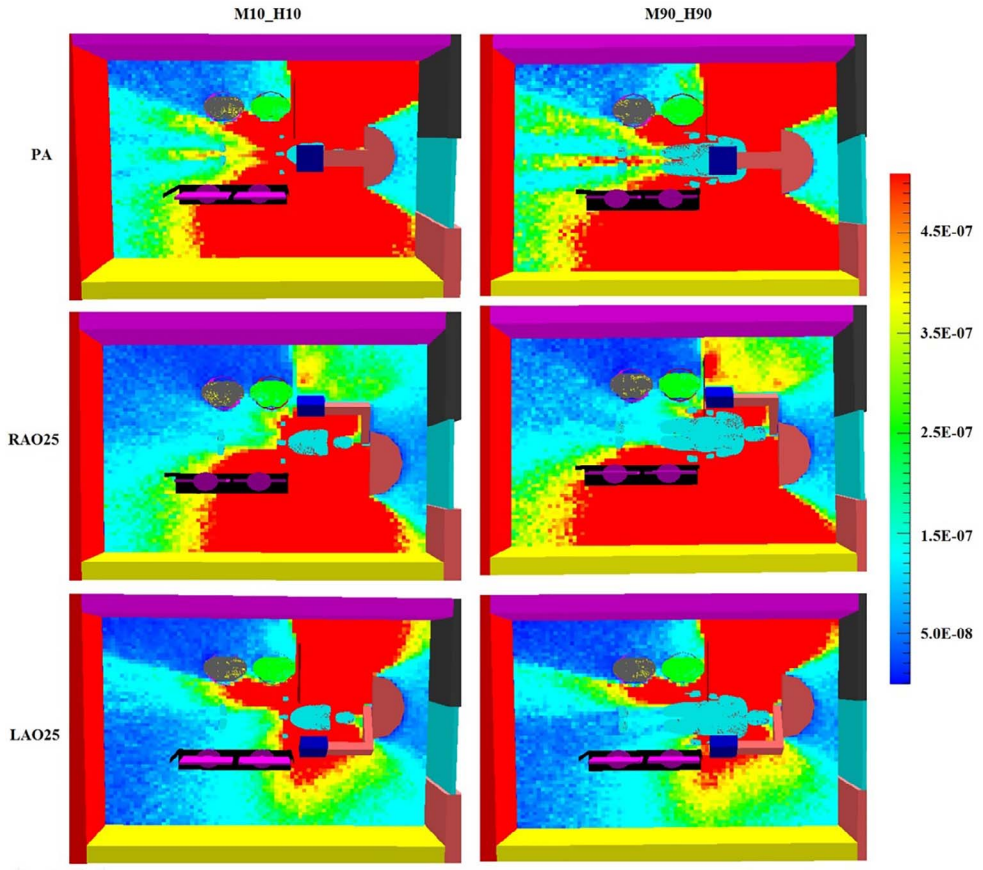

Fig. 3. Energy fluence map (MeV/cm^2), in the PTBD procedure room, as a function of the BMI of the patient.

than our results, but these cases are cardiac interventional exams.

3.2. Evaluation of CC[H_T] and CC[E] to the patient

In Table 5 the organs with the highest CC[H_T] values of the male patient are shown, with a 30 cm FOV. The complete data, for all organs, projections, gender and FOV are presented at the Supplementary Material of this paper (Tables 20–23). In most cases, the CC[H_T] to the patient rapidly increases as the patient's BMI decreases. This occurs, because the photon emitted from the patient organs and tissues may be less attenuated in the M10_H10 than in the M90_H90 phantoms. This trend was also observed in the female phantoms. With the increase of the tube voltage, the CC[H_T] of the patient also increased.

Comparing the $(E/DAP)_{Female}$ and $(E/DAP)_{Male}$ (presented at the Supplementary Material), we observed that the female presented the highest values, that were 10% (20 cm FOV, 80 kVp) to 37% (30 cm FOV, 80 kVp) higher that those of the male patient.

As stated in the ICRP 103 (p 109) [23]:

> *Effective dose can be of value for comparing the relative doses from different diagnostic procedures and for comparing the use of similar technologies and procedures in different hospitals and countries as well as the use of different technologies for the same medical examination, provided that the reference patient or patient populations are similar with regard to age and sex.*

Therefore, CC[E] to patients will also be presented in this work. Table 6 shows the CC[E] results, calculated in this study, as a function of the tube voltage and beam projection. It is noted that CC[E] values increase with the increase of the tube voltage. This is expected since the most energetic photons produce larger CC[H_T], resulting in larger CC[E].

Several general trends were observed when the patient size was modified and the radiographic technique was altered. The CC[E] to patient decreases, when the BMI increases. This is due to a reduction in shielding of the soft tissue organs.

Table 6 shows the CC[E], and average CC[E], for all projections, FOV and tube voltages, which represents the total dose during a complete procedure. To compare our results with those from the literature, we evaluated the average CC[E] to patients (20 cm FOV): 0.35 mSv/Gy. cm^2 (M10_H10) and 0.19 mSv/Gy. cm^2 (M90_H90). Our results are in agreement with those from the literature (0.18 mSv/Gy.cm^2) published by Efstathopoulos et al. [31] and by Bor et al. [32] (0.24 mSv/Gy.cm^2), for cardiac procedures.

The FOV size presented a small influence to the average CC[E] of the patient, up to 5%. An important point must be considered in this evaluation. We advise the reader to use our coefficients only for the estimative of effective doses, because in real situations, only a small part of the skin is directly irradiated. In our simulations, the CC[H_T] to the skin takes into consideration the entire body of the patient.

3.3. Influence of the PPE on the medical radiation workers

The use of shielding protection devices can also substantially reduce the exposure of workers. In this sense, an important point must be considered regarding the use of lead eyewear, lead apron, thyroid shield, lead curtain and lead glass shields. The use of these protectors allows the medical team to be partially protected from the radiation scattered by the patients. It is important to note that their use is mandatory in such procedures.

In order to evaluate their influence, we also simulated an IR procedure, without the use of such devices, for the PA, RAO25° and LAO25° projections. The simulations were carried out without the devices, separately, in order to determine their influences on the $(E/DAP)_{Male}$ (or CC[H_T]), one by one. The only exception was for the

eye lens. In this case we evaluated the CC[$H_{Eye\ lens}$] without the lead eyewear, and also without both the lead eyewear and lead glass shields. For the lead apron, we present the 5 highest variations of CC[H_T]. The results are presented in Table 7.

The results presented the highest percentage decrease of dose with PPE for the lead apron. The $(E/DAP)_{Male}$ presented a reduction of 89% and the CC[H_{Breast}] of 96%.

3.4. Energy fluence map due to the scattered radiation

To obtain an energy fluence map, we used the MCNPX mesh tally. This map was due to scattered radiation from the patient's bed. An asymmetrical distribution of scattered radiation was observed (Fig. 3). The lowest energy fluence was obtained for the RAO25° projection, in comparison with the other projections, studied in this work. This fact shows that this type of angulation will produce the lowest levels of scattered radiation to the medical radiation workers.

4. Conclusions

In this study, we used the Monte Carlo simulation, with the MCNPX code, for modeling a set of computational scenarios, to evaluate occupational exposures in PTBD procedures. The exposures were evaluated by a set of conversion coefficients, calculated based on the anthropometric characteristics of the patient, to a series of beam qualities, as a function of the DAP. The results showed that, in addition to the radiographic parameters such as tube voltage, the absorbed dose in the organs and tissues depend on the patient body weight.

From the results, it was confirmed that the CC[H_T] and CC[E] of medical radiation workers increase when the patient BMI decreases. This may be explained by the fact that the photons emitted from the organs and tissues may be less attenuated in the smaller bodies, and this increases the scattered radiation.

Nevertheless, it is important to note that the results were obtained with fixed exposure parameters, while in the actual functioning of the equipment, an increase BMI is usually associated to an automatic exposure control. If we compare M10_H10 values at 80 kVp with M90_H90 at 100 kVp, we can observe higher CC[E] values for the M90_H90 and these parameters are compatible with the clinical situation.

The use of virtual anthropomorphic phantoms of different weights and heights, to represent patients undergoing PTBD procedures, offer advantages for the understanding how body size can present an influence on medical radiation worker exposures.

Acknowledgements

The authors would like to thank Dr. Richard Kramer for kindly providing the virtual anthropomorphic phantoms used in this work. This work was partially supported by the Brazilian agencies: Fundação de Amparo à Pesquisa do Estado de Minas Gerais (FAPEMIG, Grants Nos. APQ-03049-15 and APQ-02934-15) and CNPq (Grants Nos. 304789/2011-9, 157593/2015-0, 421603/2016-0, 420699/2016-3 and 168947/2017-0).

Appendix A. Supplementary data

Supplementary data associated with this article can be found, in the online version, athttp://dx.doi.org/10.1016/j.ejmp.2017.11.016.

References

[1] Stratakis J, Damilakis J, Hatzidakis A, Theocharopoulos N, Gourtsoyiannis N. Occupational radiation exposure from fluoroscopically guided percutaneous transhepatic biliary procedures. J Vasc Interv Radiol 2006;17:863–71.
[2] Chida K, Saito H, Otani H, Kohzuki M, Takahashi S, Yamada S, et al. Relationship between fluoroscopic time, dosearea product, body weight, and maximum radiation skin dose in cardiac interventional procedures. Interventional Radiol 2006;186:774–8.
[3] Bogaert E, Bacher K, Thierens H. Interventional cardiovascular procedures in Belgium: effective dose and conversion factors. Radiat Prot Dosim 2008;129:77–82.
[4] Bozkurt A, Bor D. Simultaneous determination of equivalent dose to organs and tissues of the patient and of the physician in interventional radiology using the Monte Carlo method. Phys Med Biol 2007;52:317–30.
[5] Santos WS, Carvalho AB, Hunt JG, Maia AF. Using the Monte Carlo technique to calculate dose conversion coefficients for medical professionals in interventional radiology. Radiat Phys Chem 2014;95:177–80.
[6] Park SH, Lee JK, Lee C. Dose conversion coefficients calculated using tomographic phantom, KTMAN-2, for x-ray examination of cardiac catheterisation. Radiat Prot Dosim 2008;128:351–8.
[7] Compagnone G, Giampalma E, Domenichelli S, Renzulli M, Golfieri R. Calculation of conversion factors for effective dose for various interventional radiology procedures. Med Phys 2012;39:2491–8.
[8] Santos WS, Neves LP, Perini AP, Belinato W, Caldas LVE, Carvalho AB, Maia AF. Exposures in interventional radiology using Monte Carlo simulation coupled with virtual anthropomorphic phantoms. Physica Med 2015;31:929–33.
[9] Johnson P, Lee C, Jonhnson K, Siraqusa D, Bolch WE. The influence of patient size on dose conversion coefficients: a hybrid phantom study for adult cardiac catheterization. Phys Med Biol 2009;54:3613–29.
[10] Dauer LT, Thornton R, Boylan DC, Holahan B, Prins R, Quinn B, Germain JS. Organ and effective dose estimates for patients undergoing hepatic arterial embolization for treatment of liver malignancy. Med Phys 2011;38:736–42.
[11] Garzón WJ, Kramer R, Khoury HJ, de Barros VSM, Andrade G. Estimation of organ doses to patients undergoing hepatic chemoembolization procedures. J Radiol Prot 2015;35:629–47.
[12] Karavasilis A, Dimitriadis E, Gonis H, Pappas P, Georgiou E, Yakoumakis E. Effective dose in percutaneous transhepatic biliary drainage examination using PCXMC2.0 and MCNP5 Monte Carlo codes. Phys Med 2014;30:432–6.
[13] Neto FAB, Alves AFF, Mascarenhas YM, Nicolucci P, Pina DR. Occupational radiation exposure in vascular interventional radiology: a complete evaluation of different body regions. Physica Med 2016;32:1019–24.
[14] Neto FAB, Alves AFF, Mascarenhas YM, Giacomini G, Maués NHPB, Nicolucci P, Freitas CCM, Alvarez M, Pina DR. Efficiency of personal dosimetry methods in vascular interventional radiology. Physica Med 2017;37:58–67.
[15] Johnson PB, Geyer A, Borrego D, Ficarrotta K, Johnson K, Bolch WE. The impact of anthropometric patient-phantom matching on organ dose: a hybrid phantom study for fluoroscopy guided interventions. Med Phys 2011;38:1008–17.
[16] Cassola VF, Milian FM, Kramer R, de Oliveira Lira CA, Khoury HJ. Standing adult human phantoms based on 10th, 50th and 90th mass and height percentiles of male and female Caucasian populations. Phys Med Biol 2011;56:3749–72.
[17] Bleich SN, Bennett WL, Gudzune KA, Cooper LA. Impact of physician BMI on obesity care and beliefs. Obesity (Silver Spring) 2012;20:999–1005.
[18] Zankl M, Panzer W, Herrmann C. Calculation of patient doses using a human voxel phantom of variable diameter. Radiat Prot Dosim 2000;1–2:155–8.
[19] Tung CJ, Lee CJ, Tsai HY, Tsai SF, Chen IJ. Body size-dependent patient effective dose for diagnostic radiography. Radiat Meas 2008;43:1008–11.
[20] Cassola VF, Lima VJD, Kramer R, Khoury HJ. FASH and MASH: female and male adult human phantoms based on polygon mesh surfaces. Part II. Dosimetric calculations. Phys Med Biol 2010;55:163–89.
[21] Pelowitz DB. MCNPX User's Manual, Version 2.7.0, Report LA-CP-11-00438. Los Alamos National Laboratory; 2011.
[22] Cranley K, Gilmore B, Fogarty G, Despond L. Catalogue of diagnostic X-ray data and other data, Tech. Rep. 78. Institute of Physics and Engineering in Medicine (IPEM); 1997.
[23] ICRP Publication 103. The 2007 recommendations of the international commission on radiological protection. Ann 2007;37(24).
[24] ICRP Publication 110. 110, Adult reference computational phantoms. Ann ICRP 2009;39(2).
[25] ICRP Publication 116. Conversion coefficients for radiological protection quantities for external radiation exposures. Ann ICRP 2010;40(2-5).
[26] Tsapaki V, Kottou S, Patsilinakos S, Voudris V, Cokkinos DV. Radiation dose measurements to the interventional cardiologist using an electronic personal dosemeter. Radiat Prot Dosim 2004;112:245–9.
[27] Bor D, Onal E, Olgar T, Caglan A, Toklu T. Measurment and estimation of cardiologist dose received in interventional examinations. AAPM 48th annual meeting, Orlando, USA. 2006. pp. 1–1.
[28] Vano E, Sanchez RM, Fernandez JM. Estimation of staff lens doses during interventional procedures. comparing cardiology, neuroradiology and interventional radiology. Radiat Prot Dosim 2015;165:279–83.
[29] Martin CJ. A review of radiology staff doses and dose monitoring requirements. Radiat Prot Dosim 2009;136:140–57.
[30] Trianni A, Padovani R, Foti C, Cragnolini E, Chizzola G, Toh H, et al. Dose to cardiologists in haemodynamic and electrophysiology cardiac interventional procedures. Radiat Prot Dosim 2006;117:111–5.
[31] Efstathopoulos EP, Makrygiannis SS, Kottou S, Karvouni E, Giazitzoglou E, Korovesis S, et al. Medical personnel and patient dosimetry during coronary angiography and intervention. Phys Med Biol 2003;48:3059–68.
[32] Bor D, Sancak T, Olgar T, Elcim Y, Adanali A, Sanlidelk U, Akyar S. Comparasion of effective doses obtained from dose area product and air kerma measurements in interventional radiology. Br J Radiol 2004;77:315–22.